Received: 12 August 2019 | Revised: 6 October 2019 | Accepted: 14 October 2019

DOI: 10.1002/aoc.5328

FULL PAPER

Applied Organometallic Chemistry WILEY

Highly ordered mesoporous La(III)-substituted 5-oxopyrrolidine-2-carboxylic acid (Glp) immobilized on SBA-15 as a very efficient nanocatalyst for green aerobic oxidative coupling of thiols to disulfides

Somayeh Molaei | **Mohammad Ghadermazi**

Department of Chemistry, Faculty of Science, University of Kurdistan, Sanandaj, Iran

Correspondence
Mohammad Ghadermazi, Department of Chemistry, Faculty of Science, University of Kurdistan, Sanandaj, PO Box, 6617715175 Kurdistan, Iran.
Email: mghadermazi@yahoo.com

Funding information
University of Kurdistan

Selective aerobic oxidative coupling of thiols that are catalyzed by La(III)-substituted 5-oxopyrrolidine-2-carboxylic acid (Glp) immobilized on SBA-15 (SBA-15@Glp–La; SBA = Santa Barbara amorphous) was studied. Using SBA-15@Glp–La, the complete conversion was achieved at room temperature in the presence of air without producing any over-oxidized yields. SBA-15@Glp–La was prepared by post-grafting technique. 5-Oxopyrrolidine-2-carboxylic acid (Glp) condensation followed by La(III) impregnation caused this La(III)-grafted 5-oxopyrrolidine-2-carboxylic acid (Glp) to immobilize on SBA-15. This SBA-15@Glp–La catalyst shows excellent catalytic activity in the selective aerobic oxidative coupling of thiols. Effects of amount of the catalyst, polarity of the solvent, effects of substrate, and catalyst reusability were investigated. It has been observed that seven repetitive reaction cycles did not cause any appreciable loss in the catalytic activity of this catalyst. The catalyst characterization by scanning electron microscopy, energy-dispersive X-ray spectroscopy, X-ray diffraction, Fourier-transform infrared spectroscopy, thermal gravimetric analysis, transmission electron microscopy, inductively coupled plasma, elemental mapping, and N_2 adsorption–desorption is reported. The procedure developed is heterogeneous and environmentally benign.

KEYWORDS
aerobic oxidation, La(III) and nanoporous catalyst, thiols

1 | INTRODUCTION

Oxidative coupling of thiols is a significant procedure from both biological and synthetic viewpoints, owing to the different features of disulfide bonds, for example, as an intermediate in organic synthesis; the reaction is also important in the petroleum industry, as it is useful for the elimination of thiols by converting them into disulfides. Extensive investigations have been performed to analyze the mechanism underlying the oxidation of thiols to disulfides. However, these catalytic routes suffer from over-oxidation. The weakness of sulfur–sulfur bonds leads to over-oxidation of disulfides, which in turn results in the yield of sulfonates, sulfinates, sulfonic acids, and sulfoxides. In this regard, selective oxidation control has attracted attention as it offers some benefits,

such as less workup, short reaction time, minimum waste, and low cost.[1–6] Because of these appealing features of selective oxidation procedures, some studies have focused on the selective oxidation of thiols. Many of the catalysts used are based on manganese(III) Schiff-base complex chromium,[3] cobalt–iron magnetic composites,[5] trichlorooxyvanadium,[6] benzyltriphenylphosphonium peroxymonosulfate,[7] rhenium,[8] NaI,[9] Ni-nanoparticles,[10] potassium phosphate,[11] iodine and $CeCl_3 \cdot 7H_2O$,[12] metal–organic frameworks,[13] and lead oxide.[14] These catalytic routes involve high reaction temperatures, often toxic by-products, expensive catalysts, long reaction times, stoichiometric dosages of catalysts, and use homogeneous catalysts, and thus, have reusability problems. Some of these catalytic routes also use strong oxidants such as oxygen with high pressures and hydrogen peroxides that are dangerous in handling, storage, and transportation.[2] Therefore, it is favorable to report a heterogeneous catalytic procedure that is environmentally friendly, highly selective, and uses air as an environmentally benign, sustainable, and green oxidant.

Various elements, such as copper,[15] manganese,[4] vanadium,[6] bismuth,[16] nickel,[10] have been developed to catalyze the aerobic oxidative coupling of thiols into disulfides. Lanthanides have found great use as Lewis acids in green organic chemistry because of their availability at a moderate price, stability, and low toxicity.[17] In recent years, interest in the development of heterogeneous catalysts has increased enormously. A variety of approaches have been applied for the development of heterogeneous catalysts that usually involve the immobilization of homogeneous catalysts on the surfaces of both organic and inorganic solids, including mesoporous materials, polymers, and dendritic systems.[18–20] The ordered mesoporous materials such as SBA-15 (SBA = Santa Barbara amorphous), MCM-41, SBA-16, and MCM-48 have attracted considerable attention as supports in various catalytic applications due to their high surface area and pore volume, uniform pore size distribution, large pore size, tunable structure, and extraordinarily wide possibilities for functionalization.[21–26] Among the mesoporous silica materials, SBA-15 shows interesting textural properties, such as high hydrothermal stability, thick silica walls, and high surface-to-volume ratio.[27–32] The aim of this study was to present an environmentally benign, economical, heterogeneous catalytic process using La(III) complexes immobilized on mesoporous SBA-15 for the oxidation of thiols into the corresponding disulfides using molecular oxygen for the first time. Furthermore, air was used as an oxidizing agent, as it is more economical than pure oxygen and greener than hydrogen peroxides.

2 | EXPERIMENTAL

2.1 | Characterization

La loadings in the SBA-15@Glp–La catalyst were determined by inductively coupled plasma-optical emission spectrometry (ICP-OES; 730-ES Varian). X-ray powder diffraction (XRD) data were obtained on an MPD diffractometer (X'pert) using Cu Kα radiation (45 kV, 40 mA). The Fourier-transform infrared (FT-IR) spectra were collected with a spectrometer (VERTEX 80 model; BRUKER) using the KBr pellet technique. Thermogravimetric analyses (TGAs) were performed for the catalyst with a thermogravimetric analyzer (Shimadzu DTG 60). Scanning electron microscopy (SEM) images were obtained on FESEM-TESCAN MIRA3. Nitrogen adsorption-desorption isotherm (BET) was recorded on Volumetric adsorption analyzer Japan, BLISORP-MINI II, using a standard gas manifold at 77 K.

2.2 | SBA-15 preparation

The silica SBA-15 catalyst was synthesized according to the procedure reported previously.[33] A typical synthesis involves the following steps: pluronic P123 (4.0 g) was introduced to 30 mL of H_2O and 90 mL of HCl (2 M), and the mixture was stirred at 30 °C for 5 hr. Then, tetraethyl orthosilicate (9.04 mL, 40.78 mmol) was added dropwise and stirred for 20 hr. The white precipitate was collected and washed with distilled water. Then, the powder was dried. Afterward, the obtained powder was calcined at 823 K (5 hr).

2.3 | Immobilization of 5-oxopyrrolidine-2-carboxylic acid onto SBA-15

5-Oxopyrrolidine-2-carboxylic acid (Glp) incorporation into SBA-15 was achieved using the following procedure: pure SBA-15 (1 g) was introduced to 30 mL deionized water including 5-oxopyrrolidine-2-carboxylic acid (1.5 g, 11.61 mmol) and then refluxed (48 hr). The precipitate was collected and washed three times with distilled water. After that, the powder was dried (SBA-15@Glp).

2.4 | Synthesis of SBA-15@Glp–La catalyst

The SBA-15@Glp–La catalyst was prepared through the coordination of La(III) with the Glp ligand grafted on the SBA-15 support. Approximately 1.0 g of SBA-15@Glp

was added into 30 mL of ethanol containing 2.5 mmol of $La(NO_3)_3$ (1.08 g) and then refluxed for 16 hr. The resultant solid was collected and extensively washed with ethanol. After that, the powder was dried at 60 °C. Schematic presentation of these catalysts is displayed in Scheme 1.

2.5 | General procedure for aerobic oxidative coupling of thiols over SBA-15@Glp–La

To the SBA-15@Glp–La (5 mg) complex in ethanol (5 mL), the thiol (1 mmol) was introduced and molecular oxygen/air was simply bubbled. At room temperature, the reaction mixture was stirred and the progress of the reaction was observed with thin-layer chromatography. Then, the catalyst was collected by centrifugation. The filtrate was separated and washed several times with water. The filtrate was then separated with ethyl acetate and finally dried by evaporating of solvent to obtain a solid product.

2.6 | Selected spectral data

Dibenzyl disulfide (Table 5, Entry 3) – ^{1}H (400 MHz, $CDCl_3$, ppm): δ 3.65 (s, 4H), 7.30–7.38 (m, 10H).

1,2-Bis(4-methyl phenyl) disulfane (Table 5, Entry 9) – ^{1}H NMR (400 MHz, $CDCl_3$): δ 2.48 (s, 6H), 4.11–4.16 (m, 4H), 7.81–7.83(m, 4H) ppm.

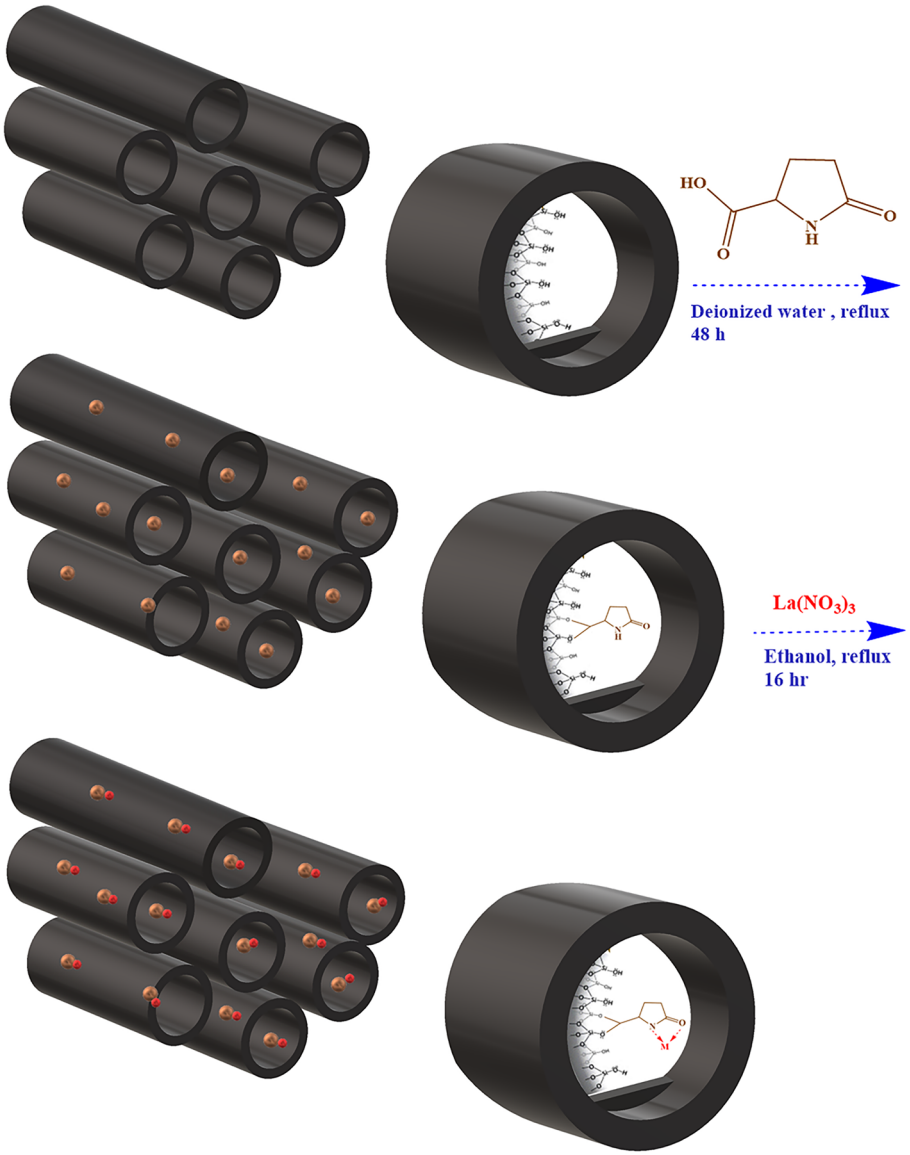

SCHEME 1 Schematic depiction of the preparation of the catalysts

3 | RESULTS AND DISCUSSION

3.1 | Low-angle XRD pattern studies

As shown in Figure 1, the low-angle XRD patterns demonstrated that the SBA-15 sample exhibited an intense (100) reflection and two weak diffraction corresponding to the (110) and (200) reflections attributable to the hexagonal mesostructure (p6mm).

A comparison of the XRD patterns of SBA-15, SBA-15@Glp–La shows that the intensity of the peak characteristic of the (100) diffraction has been decreased and the two peaks corresponding to the (110) and (200) reflections have disappeared after metal complex formation in SBA-15.

This result could be attributed to the lowering of local order, such as variations in the wall thickness, or might be due to the reduction of scattering contrast between the channel wall of the silicate framework and the La complex present in SBA-15@Glp–La.[34–36]

3.2 | N_2 adsorption–desorption studies

N_2 adsorption–desorption isotherms demonstrate that both the pristine SBA-15 and the SBA-15@Glp–La samples (Figure 2) present the typical IV type isotherms (according to the IUPAC nomenclature) with hysteresis loops, indicating that the mesoporous structure has been preserved. With immobilization of the La(III) Glp complex, hysteresis occurs at lower P/P_0 values.

Some structural parameters were calculated, on the basis of the N_2 adsorption–desorption isotherms, and are listed in Table 1. The SBA-15 has a BET surface area (A_{sBET}) of 555 m^2 g^{-1} and a primary mesopore volume

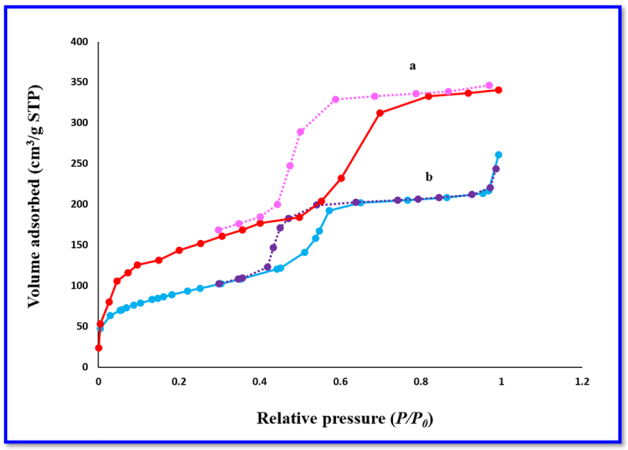

FIGURE 2 N_2 adsorption–desorption of SBA-15 (labeled a) and SBA-15@Glp–La (labeled b). STP, standard temperature and pressure

(V_p) of 0.554 cm^3 g^{-1}. The average pore diameter was calculated to be 2.4 nm for SBA-15 using the Barrett–Joyner–Halenda (BJH) method. All the calculated values were in agreement with those reported for good-quality mesoporous silica. By contrast, the SBA-15@Glp–La catalyst shows smaller N_2 uptake (BET surface area

TABLE 1 Surface exclusivity of SBA-15 and metal-grafted SBA-15

Sample	BET surface area (cm^2/g)	Pore diameter by the BJH method (nm)	Pore volume (cm^3/g)
SBA-15	555.2	2.4	0.554
SBA-15@Glp–La	321.5	1.2	0.396

[a]BET, Brunauer–Emmett–Teller; BJH, Barrett–Joyner–Halenda.

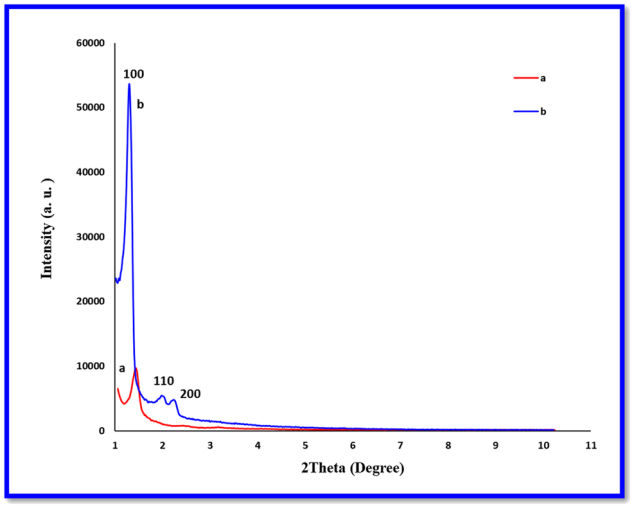

FIGURE 1 X-ray diffraction analysis of SBA-15@Glp–La (labeled a) and SBA-15 (labeled b)

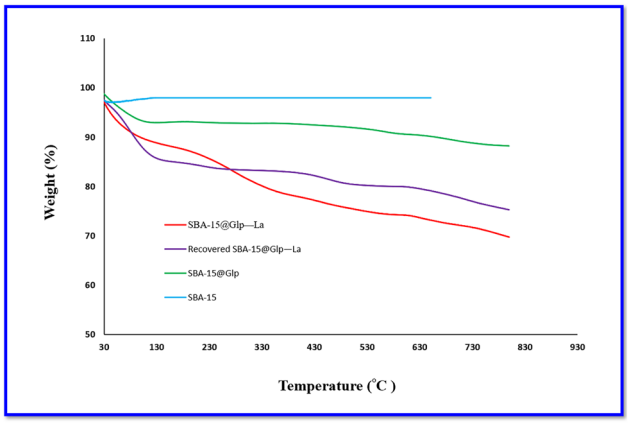

FIGURE 3 Thermogravimetric analysis curves of SBA-15, SBA-15@Glp, SBA-15@Glp–La, and recovered SBA-15@Glp–La

321 $m^2 g^{-1}$) as well as smaller pore volume (0.396 cm3 g^{-1}) and pore diameter (1.2 nm). The decrease in the BET surface area and V_p value of SBA-15@Glp–La in comparison with those of SBA-15 clearly demonstrates that the immobilization of Glp–La onto the mesoporous silica has a significant effect on pore structure of the catalyst. One of the possible reasons for this difference in the BET surface area, *Vp*, and pore diameter values between SBA-15 and SBA-15@Glp–La might be the immobilization of metal complex onto the nanosized pores of the mesoporous material.[35,37]

3.3 | Thermogravimetric studies

The TGA curves of SBA-15, SBA-15@Glp, SBA-15@Glp–La, and recovered SBA-15@Glp–La are depicted in Figure 3. In all samples the weight loss from 35 to 150 °C was assigned to the removal of adsorbed water in the mesoporous materials. The weight loss from 150 to 365 °C was assigned to the decomposition of the structure of organic groups. The weight loss from 365 to 650 °C

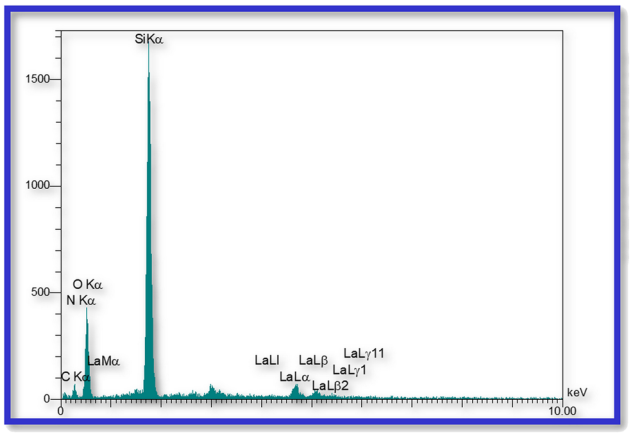

FIGURE 5 Energy-dispersive X-ray spectroscopy pattern of SBA-15@Glp–La

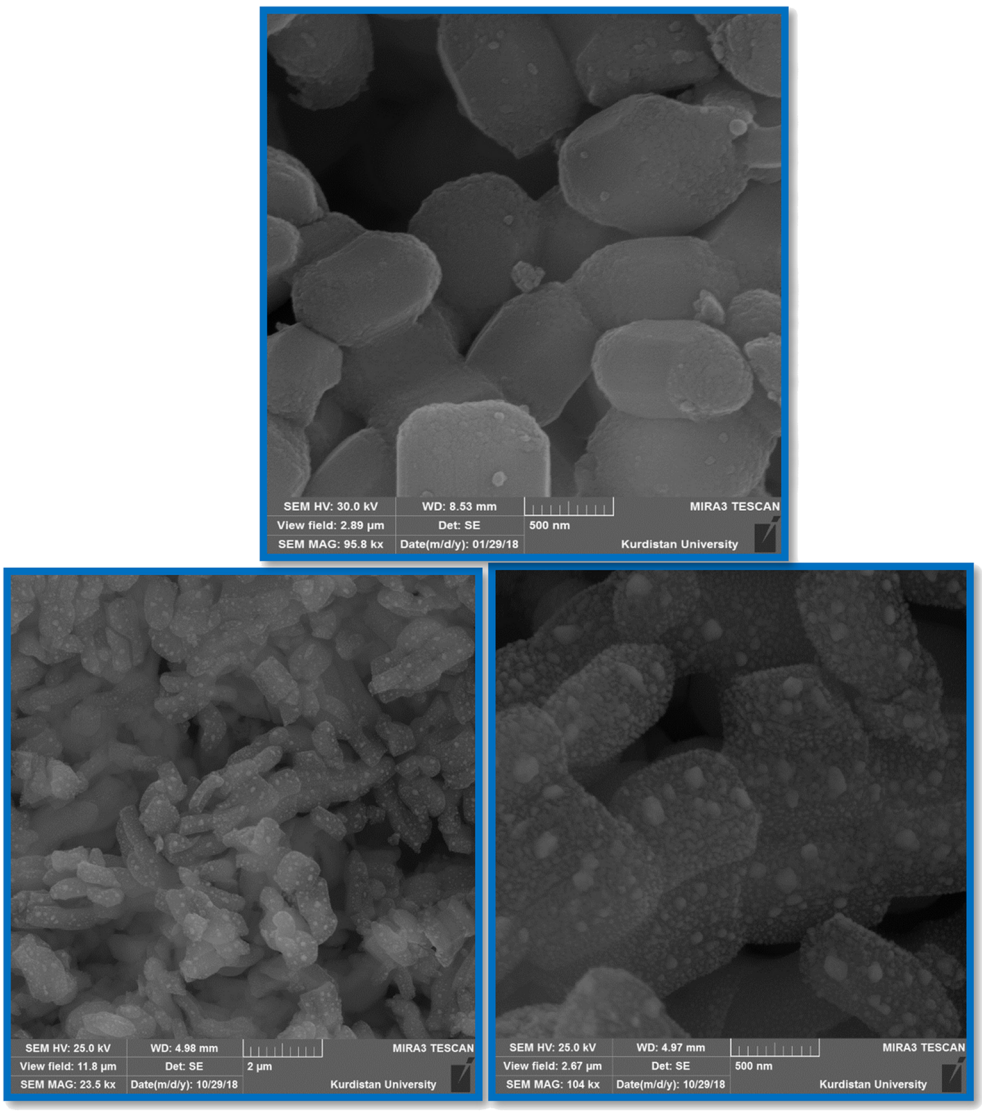

FIGURE 4 Scanning electron microscopy images of SBA-15 (top) and SBA-15@Glp–La (bottom)

was attributed to the decomposition of organic residues with high molecular weight, whereas the weight loss between 600 and 800 °C resulted from the decomposition of silanol groups.[38,39]

Therefore, in order to obtain more information about the SBA-15@Glp–La catalyst, both the support (SBA-15@Glp) and the catalyst (SBA-15@Glp–La) were treated in an N_2 atmosphere. As a result, the final decomposition temperatures for the SBA-15@Glp–La catalyst compare with SBA–15@Glp increased. This phenomenon can also be explained by the strong interaction of La(III) with organic groups that enhanced the catalyst stability, as observed for the delayed starting decomposition temperature. The TG results of the as-prepared SBA-15@Glp–La also confirmed that La(III) had a strong interaction with the Glp group. TGA analysis of reused SBA-15@Glp–La showed a mass loss between 200 and 600 °C, which corresponds to the removal of organic moieties.

3.4 | SEM photographs, energy-dispersive X-ray analysis, and elemental mapping

Figure 4 shows the SEM of the SBA-15 and SBA-15@Glp–La at different magnetization. It can be observed that SBA-15@Glp–La has a pipe-like domain morphology. Furthermore, the SEM measurements indicate that a similar morphology can be seen in the SBA-15-functionalized sample. Energy-dispersive X-ray analysis of SBA-15@Glp–La shows the existence of silicon, oxygen, carbon, nitrogen, and La in the catalyst and the spectrum is depicted in Figure 5. As shown in Figure 6, the elemental mapping confirmed a homogeneous distribution of silicon, oxygen, carbon, nitrogen, and La in the SBA-15@Glp–La catalyst. Finally, the amount of La(III) in the catalyst was estimated using ICP-OES to be 0.32 mmol g^{-1}.

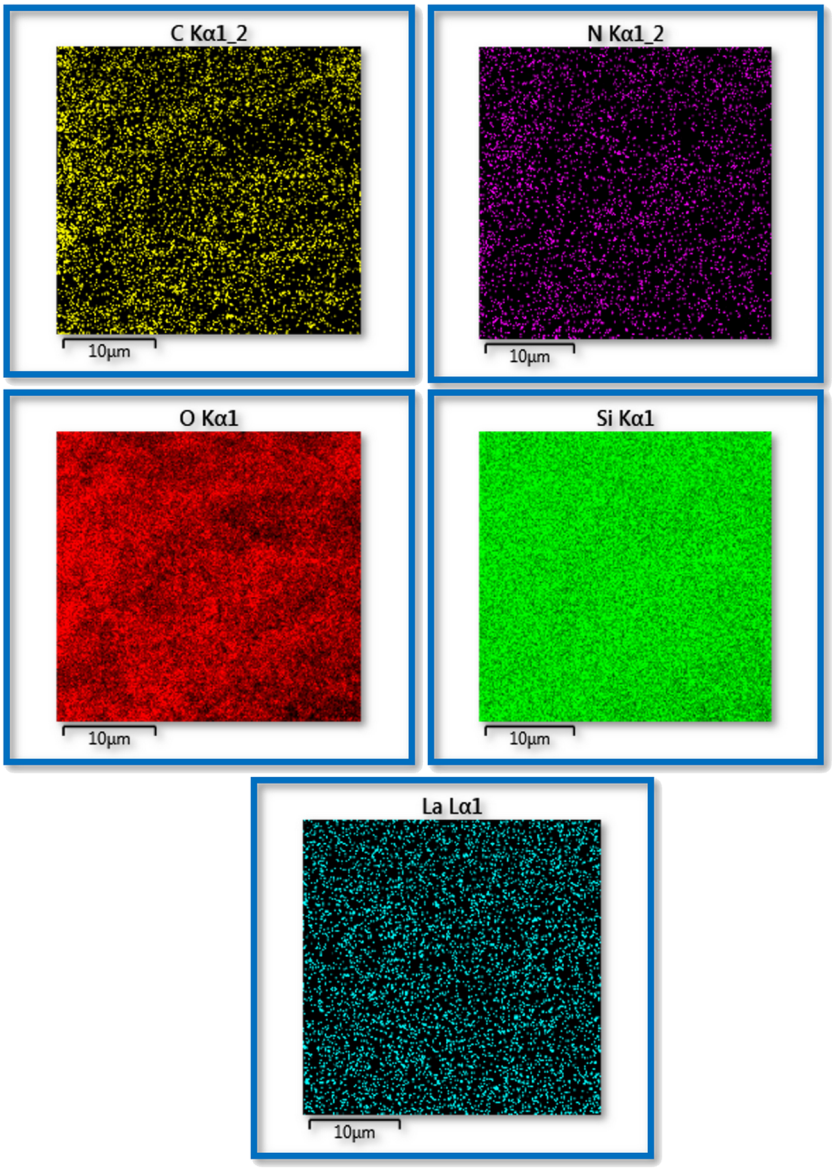

FIGURE 6 Elemental mapping images of SBA-15@Glp–La

3.5 | FT-IR spectra

The FT-IR spectra of SBA-15, SBA-15@Glp, SBA-15@Glp–La, and reused SBA-15@Glp–La are shown in Figure 7. The FT-IR spectra of siliceous materials, containing asymmetric Si–O–Si stretching at 1082 cm^{-1}, symmetric Si–O–Si stretching at 806 cm^{-1}, and bending Si–O–Si vibration at 463 cm^{-1} were seen in the FT-IR spectra of all samples, indicating that the silica framework remains unaffected upon modification. The FT-IR spectrum of the SBA-15@Glp sample shows bands around 1639 and 1383 cm^{-1}, which can be assigned to the C=O stretching vibration and the C–N stretching vibration, respectively, indicating the successful attachment of the Glp groups onto the solid surface SBA-15 support. The FT-IR spectrum of the SBA-15@Glp–La sample (Figure 7, c) shows the band for the C=O stretching vibration at 1635 cm^{-1}, which has been shifted to a lower wavenumber, showing that C=O groups are coordinated to La(III) species. The FT-IR spectrum of the reused SBA-15@Glp–La sample (Figure 7, d) shows that the structure of the catalyst has remained unchanged even after seven runs. The FT-IR spectrum of reused catalyst indicated that it can be recycled seven times without significant change in the structure of silicate.

3.6 | TEM images

The TEM image of SBA-15@Glp–La (Figure 8) shows the presence of ordered mesostructures in this sample. The TEM micrograph of SBA-15@Glp–La viewed along the pore axis reveals a hexagonal array. The TEM image provides strong evidence that the long-range ordering of the support framework is retained even after the immobilization of the La(III)–Glp complex in the mesoporous silica matrix. These data indicate that the immobilization of the La(III)–Glp complex has taken place substantially inside the pore channels of SBA-15.

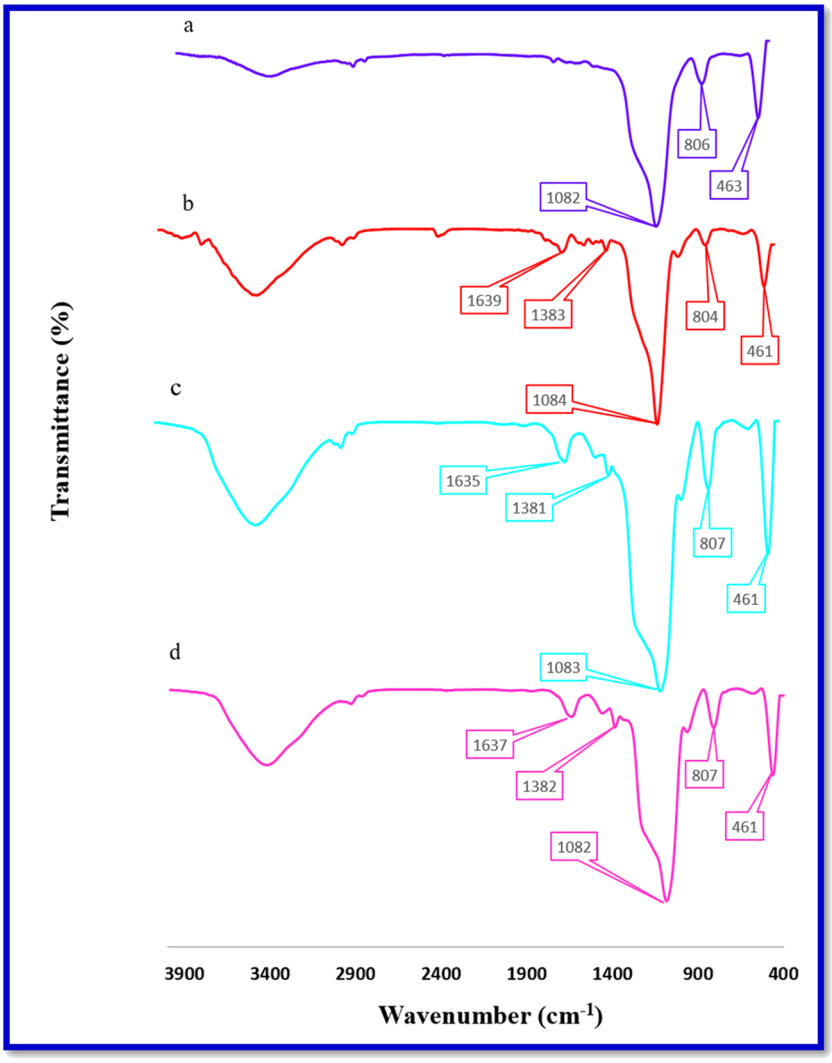

FIGURE 7 Fourier-transform infrared spectra of SBA-15 (labeled a), SBA-15@Glp (labeled b), SBA-15@Glp–La (labeled c), and recovered SBA-15@Glp–La (labeled d)

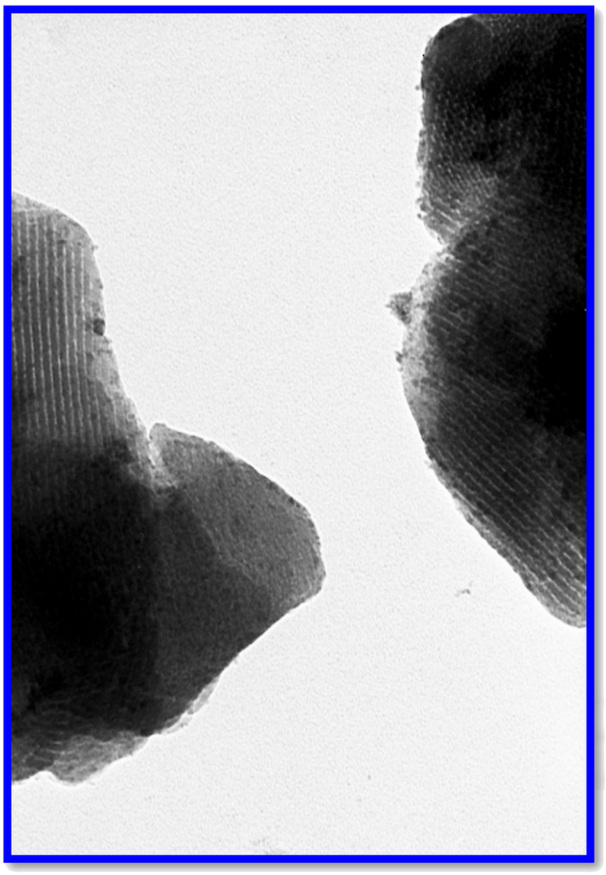

FIGURE 8 Transmission electron microscopy images of SBA-15@Glp–La

3.7 | Catalytic studies

The SBA-15@Glp–La catalyst has been used for the aerobic oxidation of thiols to disulfides. We performed a test to confirm that the catalytic performance of SBA-15@Glp–La originates from the immobilized La sites (Table 2). 4-methylthiophenol was chosen as a substrate to perform this control test. We have performed the oxidation of 4-methylthiophenol using SBA-15 and SBA-15@Glp as catalysts in ethanol at room temperature, but in these cases, no reaction occurs after 2 hr. Then, the aerobic oxidation of thiol was performed using homogeneous-phase $La(NO_3)_3$ as the catalyst (Table 2, Entry 3). The conversion of 4-methylthiophenol was 80%. It is evident that the presence of La is essential for this transformation. However, it cannot be reused due to the homogenous nature of the $La(NO_3)_3$. After that, the

TABLE 2 Testing of various catalysts for oxidation of 4-methylthiophenol[a]

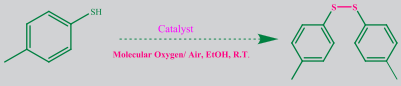

Entry	Catalyst	Time	Yield (%)[b]
1	SBA-15	2 hr	0
2	SBA-15@Glp	2 hr	0
3	$La(NO_3)_3$	2 hr	80
4	La supported over SBA-15	2 hr	85
5	SBA-15@Glp–La	15 min	91

[a]Reaction conditions: 4-methylthiophenol (1 mmol), catalyst (6 mg), r.t. (room temperature).
[b]Isolated yield of product.

TABLE 3 Effect of various solvents on the oxidative coupling of thiol using 4-methylthiophenol with molecular oxygen/air as oxidant and SBA-15@Glp–La as catalyst[a]

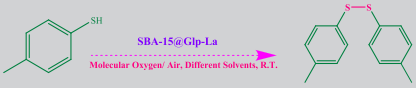

Entry	Solvent	Time (min)	Yield (%)[b]
1	*n*-Hexane	45	72
2	Dichloromethane	35	78
3	Ethyl acetate	30	84
4	Acetonitrile	25	88
5	EtOH	20	92

[a]Reaction conditions: thiol (1 mmol), catalyst (6 mg), and solvent (3 mL) at room temperature (r.t.).
[b]Isolated yield.

TABLE 4 Effect of catalyst dosage on the oxidative coupling of thiol using 4-methylthiophenol with molecular oxygen/air as oxidant and SBA-15@Glp–La as catalyst[a]

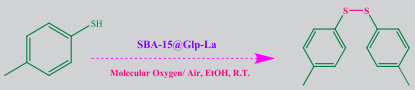

Entry	Catalyst (mg)	Time	Yield (%)[b]
1	0	10 hr	Trace
2	2	45 min	80
3	4	30 min	87
4	6	20 min	92
5	8	15 min	93
6	10	12 min	94
7	12	10 min	94

[a]Reaction conditions: thiol (1 mmol), catalyst, and EtOH (3 mL) at room temperature (r.t.).
[b]Isolated yield.

TABLE 5 The catalytic efficiency of SBA-15@Glp–La in the oxidation of thiols[a]

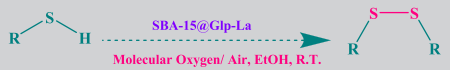

Entry	Substrate	Product	Time (min)	Yield (%)2	Melting point (°C)
1	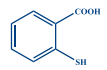	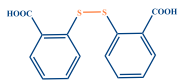	35	91	275–282[40]
2		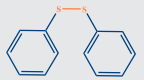	30	92	58–60[10]
3	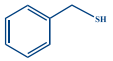	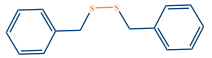	22	94	66–71[40]
4	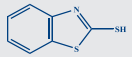	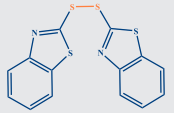	13	96	175–176[41]
5	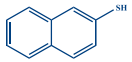	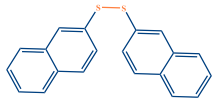	17	94	133–135[41]
6			20	92	Oil[41]

(Continues)

TABLE 5 (Continued)

Entry	Substrate	Product	Time (min)	Yield (%)2	Melting point (°C)
7	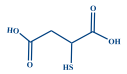	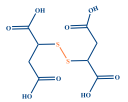	25	93	105–108[42]
8	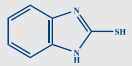	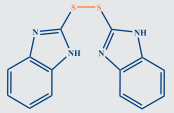	16	91	199–201[42]
9	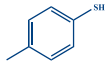	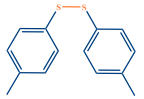	20	92	37–42[43]
10	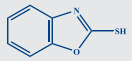	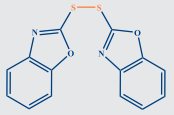	15	95	78–84[43]

[a]Reactions conditions: thiol (1 mmol), catalyst (6 mg), and molecular oxygen/air as oxidant.
[b]Isolated yield.

aerobic oxidation of 4-methylthiophenol was carried out by La-immobilized SBA-15, after which the conversion increased a little. By contrast, when the aerobic oxidation of 4-methylthiophenol was performed in the presence of SBA-15@Glp–La as the catalyst, the yield increased remarkably. Large surface area enables organic molecules to diffuse into the channel of SBA-15 and helps them interact with $La(NO_3)_3$. This explains why the rate of aerobic oxidation of 4-methylthiophenol in the presence of SBA-15@Glp–La is quite higher than other conventional catalysts.

In the second part of the study, thiols were oxidized to disulfides in different solvents under aerobic condition using SBA-15@Glp–La as the catalyst. 4-Methylthiophenol was selected as the model substrate. The results are presented in Table 3. *n*-Hexane, dichloromethane, ethyl acetate, acetonitrile, and ethanol were tested as solvents in the reaction. The non-polar solvent *n*-hexane provided the lowest conversion, whereas polar aprotic solvents such as dichloromethane, EtOAc, and CH_3CN gave 78%, 84%, and 88% conversion, respectively. When the polar protic solvent EtOH was utilized, 92% conversion was achieved. In polar aprotic acetonitrile, with low basicity, 4-methylthiophenol reacted slowly (Table 3, Run 4). In ethanol, with high basicity, 4-methylthiophenol proceeded to react easily.

The influence of catalyst dosage on the oxidative coupling of 4-methylthiophenol was investigated. Catalyst dosage was changed from 0 to 15 mg, with the increase in catalyst dosage increasing the conversion (Table 4). The reaction, however, did not proceed in the absence of any catalyst. In fact, more amount of catalyst could offer more reactive sites for the same amount of substrate.

Next, selective aerobic oxidative coupling of various thiols catalyzed by SBA-15@Glp–La was investigated

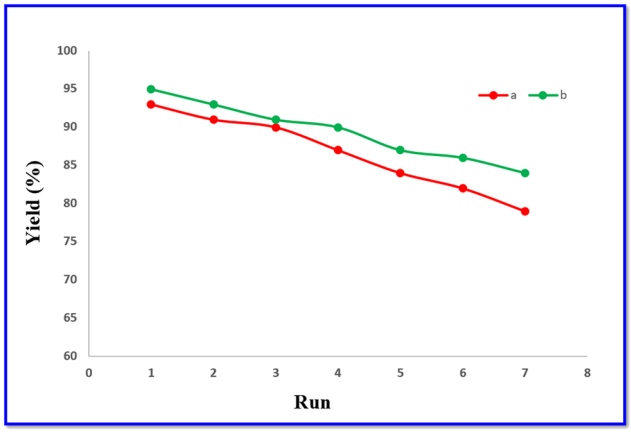

FIGURE 9 Effect of recycling of SBA-15@Glp–La on catalytic oxidative coupling of mercaptosuccinic acid (labeled a, red line) and benzo[d]oxazole-2-thiol (labeled b, green line)

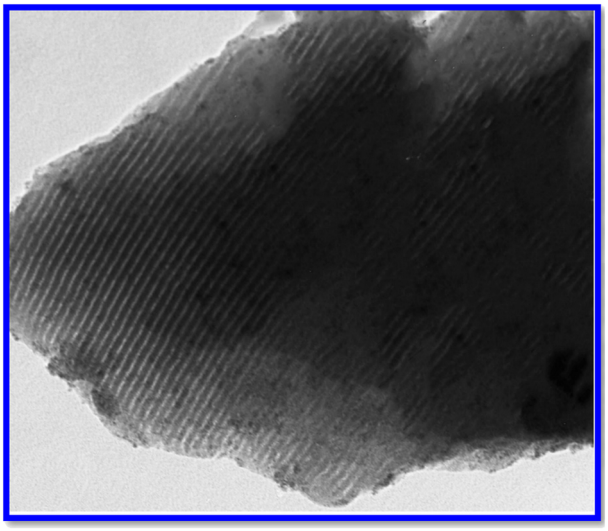

FIGURE 11 Transmission electron microscopy images of reused SBA-15@Glp–La

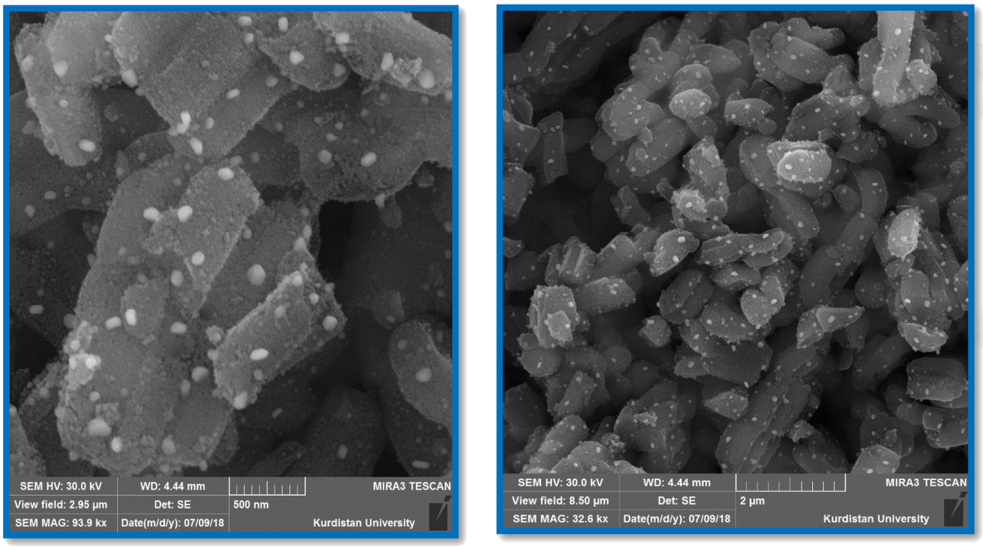

FIGURE 10 Scanning electron microscopy images of recovered SBA-15@Glp–La

(Table 5). Thiophenols having electron-donating groups, such as 4-methylthiophenol, showed oxidation at high rates. The reaction of thiols with electron-withdrawing groups showed oxidation at low rates. Many nucleophilic compounds are more active to attack La(III) species. All these reactions gave corresponding disulfides in excellent yields under mild conditions.

3.8 | Recyclability of the catalyst

To investigate the recyclability of the SBA-15@Glp–La catalyst, aerobic oxidation of mercaptosuccinic acid and benzo[d]oxazole-2-thiol to their corresponding disulfides was studied (Figure 9). The catalyst was isolated by centrifugation after the reaction. The recovered catalyst was then washed with acetone and dried in an oven. For the SBA-15@Glp–La catalyst, a small decrease of the yield was noted after seven runs. The SEM images of the recovered SBA-15@Glp–La (Figure 10) are identical to those of fresh SBA-15@Glp–La, which indicated that the novel catalysts have excellent mechanical property. The TEM image of reused SBA-15@Glp–La (Figure 11) indicates that the catalyst can be reused for seven runs without any significant change in the mesoporosity.

3.9 | Hot filtration study

A hot filtration test was performed with mercaptosuccinic acid as the model substrate under optimized condition. In the half time of the reaction, only 55% conversion was achieved. Then the aerobic oxidation of benzo[d]oxazole-2-thiol was repeated under similar reaction conditions and in half time of the reaction

TABLE 6 Comparison of SBA-15@Glp–La catalysts for the oxidative coupling of 4-methylthiophenol and thiophenol with some recently reported catalysts

Entry	Substrate	Catalyst	Solvent	Temperature (°C)	Time	Yield (%)
1	4-Methylthiophenol	K-OMS-2	Acetonitrile	100	30 min	100[2]
2	4-Methylthiophenol	Nickel nanoparticles	Acetonitrile	r.t.[a]	9 min	98[10]
3	4-Methylthiophenol	CoTSPc/SiO_2	EtOAc	r.t.	90 min	97[44]
4	4-Methylthiophenol	$VOCl_3$	EtOAc	r.t.	20 hr	96[6]
5	4-Methylthiophenol	Cu/DH	Ethanol	70	2.5 hr	<99[15]
6	4-Methylthiophenol	Mn–ZSM-5 (MZ-1RC)	Ethanol	70	6 hr	83[4]
7	4-Methylthiophenol	Diaryl telluride	CH_2Cl_2	0	15 min	99[1]
8	4-Methylthiophenol	Cobalt–iron magnetic composites	Dimethylformamide	25	1 hr	100[5]
9	4-Methylthiophenol	Manganese(III) Schiff-base complex	CH_3OH	25	17 min	97[3]
10	**4-Methylthiophenol**	**SBA-15@Glp–La**	**Ethanol**	**r.t.**	**20 min**	**92 (this work)**
11	Thiophenol	K-OMS-2	Acetonitrile	100	30 min	61[2]
12	Thiophenol	Nickel nanoparticles	Acetonitrile	r.t.	6 min	98[10]
13	Thiophenol	CoTSPc/SiO_2	EtOAc	r.t.	90 min	98[44]
14	Thiophenol	$VOCl_3$	EtOAc	r.t.	52 hr	93[6]
15	Thiophenol	Cu/DH	Ethanol	70	4 hr	<99[15]
16	Thiophenol	Mn–ZSM-5 (MZ-1RC)	Ethanol	70	6 min	84[4]
17	Thiophenol	Diaryl telluride	CH_2Cl_2	r.t.	15 min	Quant[1]
18	Thiophenol	Cobalt–iron magnetic composites	Dimethylformamide	25	3 hr	100[5]
19	Thiophenol	Manganese(III) Schiff-base complex	CH_3OH	25	18 min	98[3]
20	**Thiophenol**	**SBA-15@Glp–La**	**Ethanol**	**r.t.**	**30 min**	**92 (this work)**

Note: the entries of 10 and 20 were bold because these are our work compare with other works.

[a]Room temperature.

the catalyst was separated. However, no further increase in product conversion was observed and the yield of the reaction was 62%. This experimental result suggests no leaching of La during the reaction.

3.10 | Comparison of the catalyst

The catalytic efficiency of SBA-15@Glp–La during aerobic oxidation of 2-mercaptobenzoic acid was compared with several of the recently reported catalysts (Table 6).

4 | CONCLUSIONS

In summary, we present a very active and environmentally benign process for the selective aerobic oxidative coupling of thiols under mild reaction conditions. In the presence of SBA-15@Glp–La as heterogeneous catalyst, 100% selectivity and complete conversion at room temperature were achieved. The catalyst could be recycled after the reaction without notable reduction in catalytic performance. The non-caustic waste by-product and simplicity of the operation are appealing features of this new process.

ACKNOWLEDGEMENTS

We are grateful to Erfan Ghadermazi and the University of Kurdistan for support of this work.

ORCID

Somayeh Molaei https://orcid.org/0000-0001-6040-4830
Mohammad Ghadermazi https://orcid.org/0000-0001-8631-6361

REFERENCES

[1] M. Oba, K. Tanaka, K. Nishiyama, W. Ando, *J. Org. Chem.* **2011**, *76*, 4173.
[2] S. Dharmarathna, C. K. King'ondu, L. Pahalagedara, C.-H. Kuo, Y. Zhang, S. L. Suib, *Appl. Catal. B Environ.* **2014**, *147*, 124.
[3] H. Golchoubian, F. Hosseinpoor, *Catal. Comm.* **2007**, *8*, 697.
[4] A. K. Patra, A. Dutta, M. Pramanik, M. Nandi, H. Uyama, A. Bhaumik, *ChemCatChem* **2014**, *6*, 220.
[5] L. Menini, M. C. Pereira, A. C. Ferreira, J. D. Fabris, E. V. Gusevskaya, *Appl. Catal., a* **2011**, *392*, 151.
[6] M. Kirihara, K. Okubo, T. Uchiyama, Y. Kato, Y. Ochiai, S. Matsushita, A. Hatano, K. Kanamori, *Chem. Pharm. Bull.* **2004**, *52*, 625.
[7] A. R. Hajipour, S. E. Mallakpour, H. Adibi, *J. Org. Chem.* **2002**, *67*, 8666.
[8] J. B. Arterburn, M. C. Perry, S. L. Nelson, B. R. Dible, M. S. Holguin, *J. Am. Chem. Soc.* **1997**, *119*, 9309.
[9] M. Kirihara, Y. Asai, S. Ogawa, T. Noguchi, A. Hatano, Y. Hirai, *Synthesis* **2007**, *2007*, 3286.
[10] A. Saxena, A. Kumar, S. Mozumdar, *J. Mol. Catal. Chem.* **2007**, *269*, 35.
[11] A. V. Joshi, S. Bhusare, M. Baidossi, N. Qafisheh, Y. Sasson, *Tetrahedron Lett.* **2005**, *46*, 3583.
[12] C. C. Silveira, S. R. Mendes, *Tetrahedron Lett.* **2007**, *48*, 7469.
[13] A. Dhakshinamoorthy, M. Alvaro, H. Garcia, *Chem. Commun.* **2010**, *46*, 6476.
[14] J. P. Nehlsen, J. B. Benziger, I. G. Kevrekidis, *Energy Fuels* **2004**, *18*, 721.
[15] A. Dhakshinamoorthy, S. Navalon, D. Sempere, M. Alvaro, H. Garcia, *ChemCatChem* **2013**, *5*, 241.
[16] Y. P. Bhoi, D. P. Rout, B. G. Mishra, *J. Cluster Sci.* **2016**, *27*, 267.
[17] M. Oliverio, M. Nardi, P. Costanzo, L. M. Di Gioia, A. Procopio, *Sustainability*. **2018**, *10*, 721.
[18] L. Zhu, X.-Q. Liu, H.-L. Jiang, L.-B. Sun, *Chem. Rev.* **2017**, *117*, 8129.
[19] G. Kyriakou, S. K. Beaumont, R. M. Lambert, *Langmuir* **2011**, *27*, 9687.
[20] M. Yoon, R. Srirambalaji, K. Kim, *Chem. Rev.* **2012**, *112*, 1196.
[21] Y. Zhang, S. N. Riduan, *Chem. Soc. Rev.* **2012**, *41*, 2083.
[22] D. Borisova, H. Möhwald, D. G. Shchukin, *ACS Nano* **2011**, *5*, 1939.
[23] B. G. Trewyn, I. I. Slowing, S. Giri, H.-T. Chen, V. S. Y. Lin, *Acc. Chem. Res.* **2007**, *40*, 846.
[24] W. Chen, P.-H. Tsai, Y. Hung, S.-H. Chiou, C.-Y. Mou, *ACS Nano* **2013**, *7*, 8423.
[25] F. Hoffmann, M. Cornelius, J. Morell, M. Fröba, *Angew. Chem.* **2006**, *45*, 3216.
[26] S. Molaei, T. Tamoradi, M. Ghadermazi, A. Ghorbani-Choghamarani, *Catal. Lett.* **2018**, *148*, 1834.
[27] N. Lashgari, A. Badiei, G. Mohammadi Ziarani, *Nanochem Res.* **2016**, *1*, 127.
[28] C. Li, Y. Wang, Y. Guo, X. Liu, Y. Guo, Z. Zhang, Y. Wang, G. Lu, *Chem. Mater.* **2007**, *19*, 173.
[29] R. Huirache-Acuña, R. Nava, L. C. Peza-Ledesma, J. Lara-Romero, G. Alonso-Núez, B. Pawelec, M. E. Rivera-Muñoz, *Materials.* **2013**, *6*, 4139.
[30] Y. Znamenskaya, S. Björklund, V. Kocherbitov, V. Alfredsson, *Micropor. Mesopor. Mat.* **2016**, *230*, 58.
[31] S. Molaei, T. Tamoradi, M. Ghadermazi, A. Ghorbani-Choghamarani, *Polyhedron* **2018**, *156*, 35.
[32] S. Molaei, T. Tamoradi, M. Ghadermazi, A. Ghorbani-Choghamarani, *Appl. Organomet. Chem.* **2019**, *33*, e4649.
[33] J. Davarpanah, A. R. Kiasat, *Catal. Comm.* **2014**, *46*, 75.
[34] J. Huang, M. Wang, S. Zhang, B. Hu, H. Li, *J. Phys. Chem. C* **2011**, *115*, 22514.
[35] H. Li, F. Zhang, Y. Wan, Y. Lu, *J. Phys. Chem. B.* **2006**, *110*, 22942.
[36] F. Wang, L. Jiang, J. Wang, Z. Zhang, *Energy Fuels* **2016**, *30*, 5885.
[37] Y. Zhang, Q. Xiong, Y. Chen, M. Liu, P. Jin, Y. Yan, J. Pan, *Ind. Eng. Chem. Res.* **2018**, *57*, 1968.
[38] S. M. Rivera-Jiménez, S. Méndez-González, A. Hernández-Maldonado, *Micropor. Mesopor. Mat.* **2010**, *132*, 470.
[39] M. Khanmoradi, M. Nikoorazm, A. Ghorbani-Choghamarani, *Appl. Organomet. Chem.* **2017**, *31*, e3693.

[40] T. Tamoradi, A. Ghorbani-Choghamarani, M. Ghadermazi, *New J. Chem.* **2017**, *41*, 11714.
[41] T. Tamoradi, M. Ghadermazi, A. Ghorbani-Choghamarani, *Appl. Organomet. Chem.* **2018**, *32*, e3974.
[42] S. Molaei, T. Tamoradi, M. Ghadermazi, A. Ghorbani-Choghamarani, *Micropor. Mesopor. Mat.* **2018**, *272*, 241.
[43] T. Tamoradi, B. Mehraban-Esfandiari, M. Ghadermazi, A. Ghorbani-Choghamarani, *Res. Chem. Intermed.* **2018**, *44*, 1363.
[44] A. Shaabani, N. Safari, S. Shoghpour, A. H. Rezayan, *Monatsh. Chem.* **2008**, *139*, 613.

How to cite this article: Molaei S, Ghadermazi M. Highly ordered mesoporous La(III)-substituted 5-oxopyrrolidine-2-carboxylic acid (Glp) immobilized on SBA-15 as a very efficient nanocatalyst for green aerobic oxidative coupling of thiols to disulfides. *Appl Organometal Chem*. 2019;e5328. https://doi.org/10.1002/aoc.5328